

## Vortex dynamics and defects in simulated flux flow

M. C. Faleski, M. C. Marchetti, and A. A. Middleton

*Physics Department, Syracuse University, Syracuse, New York 13244*

(Received 8 May 1996)

We present the results of molecular dynamic simulations of a two-dimensional vortex array driven by a uniform current through random pinning centers at zero temperature. We identify two types of flow of the driven array near the depinning threshold. For weak disorder the flux array contains few dislocation and moves via correlated displacements of patches of vortices in a *crinkle* motion. As the disorder strength increases, we observe a crossover to a spatially inhomogeneous regime of *plastic* flow, with a very defective vortex array and a channel-like structure of the flowing regions. The two regimes are characterized by qualitatively different spatial distributions of vortex velocities. In the crinkle regime the distribution of vortex velocities near threshold has a single maximum that shifts to larger velocities as the driving force is increased. In the plastic regime the distribution of vortex velocities near threshold has a clear bimodal structure that persists upon time averaging the individual velocities. The bimodal structure of the velocity distribution reflects the coexistence of pinned and flowing regions and is proposed as a quantitative signature of plastic flow. [S0163-1829(96)01241-6]

### I. INTRODUCTION

The problem of nonlinear collective transport through random media has attracted much theoretical and experimental attention due to the interesting spatiotemporal phenomena that arise in a variety of physical systems from the competition between interactions and disorder. In particular, the dynamics of driven elastic media that are distorted by disorder, but cannot “break,” has been studied extensively, both theoretically and numerically. At zero temperature these systems exhibit a sharp depinning transition from a pinned state below a critical driving force  $F_c$  to a sliding state above  $F_c$ . The transition can be described as a critical phenomenon in terms of scaling laws and critical exponents. The elastic medium model can be used to describe the dynamics of weakly pinned Abrikosov flux lattices,<sup>1</sup> fronts of wetting fluids invading porous media,<sup>2</sup> and charge density waves (CDW’s) in anisotropic conductors<sup>3,4</sup> over a wide range of length scales. It is, however, expected to eventually break down (particularly in lower dimensionality) at short length scales since it yields unphysical regions of unbounded strains.<sup>5</sup> In addition, the elastic model is inadequate for many physical systems with strong disorder that exhibit a spatially inhomogeneous plastic response without long-wavelength elastic restoring forces. These include strongly pinned flux lattices,<sup>6–8</sup> invasion of nonwetting fluid in porous media,<sup>2</sup> Wigner solids in two-dimensional electron gas (2DEG), and fluid flow down a rough incline.<sup>9</sup> In these systems the competition between drive and disorder generates topological defects (dislocations, phase slips) in the medium that can qualitatively change the dynamics.<sup>10–12</sup> Collective transport in the presence of topological defects is still poorly understood.

Magnetic flux arrays in type-II superconductors are an ideal system for investigating nonlinear collective transport since by changing the applied magnetic field one can tune the strength of the intervortex interaction and observe a crossover from a regime of weak pinning, well described by collective flux creep theories, to a regime of strong pinning

with spatially inhomogeneous flow.<sup>1</sup> Evidence for this comes from early simulations of two-dimensional flux lattices by Jensen *et al.*<sup>7</sup> and by Shi and Berlinsky.<sup>8</sup> In addition, a variety of transport phenomena observed recently in superconductors has been attributed to the inhomogeneous plastic response of the flux array, including a nonmonotonic dependence of the critical current on temperature just below the flux lattice melting point (peak effect), an unusual current and field dependence of  $1/f$  broadband noise, and fingerprint phenomena.<sup>6,13–15</sup> On the other hand, the experiments only probe flux motion indirectly through transport measurements. For this reason their interpretation is difficult and still controversial. Numerical work can therefore be very valuable to gain insight into this complex problem and to serve as a guide for future theoretical work.

In this paper we report on simulations of the dynamics of a two-dimensional Abrikosov flux array driven by a uniform current through random pinning centers at zero temperature. The focus of our work, which distinguishes it from previous numerical work on the same<sup>7,8,11,16</sup> or closely related<sup>9,17,18</sup> systems, is on identifying various types of flow and establishing a connection between the type of flow or response (“elastic” versus “plastic”) and the presence of flux lattice defects and the shape of the macroscopic response as embodied, for instance, in the  $V$ - $I$  characteristics. This will be very useful for the interpretation of experiments. While most of the results presented here are somewhat qualitative, our long-term objective is to carry out simulations for realistic parameter values that will allow a detailed comparison with experiments. It is well known that short-wavelength defects, such as dislocations, play a more important role in two, rather than in three, dimensions.<sup>19</sup> For this reason many of our results will not apply directly to three-dimensional flux arrays. On the other hand, the study of two-dimensional systems is valuable both because of intrinsic interest and because in many experimental situations the flux arrays can effectively be modeled as two dimensional. Thermal fluctuations are generally important in flux flow experiments and purely dy-

namical phenomena associated with the current-induced depinning of the vortices cannot be dissociated from thermal-induced softening of the lattice. In this paper we specifically consider the flux array dynamics at  $T=0$  with the objective of disentangling these two effects.

Below we present the results of simulations of a driven flux array for both a low density and a very high density of point pinning centers. In both cases we identify two types of response or flow of the flux array near the depinning threshold and a crossover from one type to another as the disorder strength is increased. For sufficiently weak disorder the flux array contains very few defects and moves via correlated displacements of patches of vortices. The dynamics is similar to that observed by Hu and Westervelt<sup>20</sup> in magnetic bubble arrays. Following these authors' suggestion, we refer to this type of response as *crinkle* motion. For stronger disorder the response near threshold is *plastic*, with vortices flowing around pinned regions. The flux lattice is very defective and we observe channels of liquidlike vortex array flowing around solidlike pinned regions. The topology of the channels is not, however, fixed in time. Channels open and close continuously as the flux array is driven over the impurities and all vortices participate in the motion at one time or another near threshold. As the disorder is further increased the individual channels become longer lived and for very strong disorder we observe a filamentary structure with a fraction of vortices that never move on the time scale of the simulation. To characterize the different regimes we have studied in detail the spatial distribution of vortex velocities. In the crinkle regime the distribution of vortex velocity near threshold shows a single maximum corresponding roughly to the average velocity of the array, though at any time some vortices are moving with velocity significantly greater than the average value. The plastic flow regime is characterized by bimodal velocity distributions near threshold, indicating that the velocity is spatially inhomogeneous, with both pinned and flowing regions. We discuss the correlation between these qualitative features of the velocity distribution and the shape of the macroscopic  $V$ - $I$  characteristic and suggest that the shape of the velocity distribution may be used for a crude classification of the type of response.

## II. MODEL

The specific model considered here is essentially the same as that studied in earlier simulations by Jensen *et al.*,<sup>7</sup> by Shi and Berlinsky,<sup>8</sup> and, more recently, by Koshelev and Vinokur.<sup>11</sup> The two-dimensional pancake vortices are modeled as point particles with finite-range interaction and overdamped dynamics, driven through randomly placed pinning centers by a uniform force  $\mathbf{F}$  proportional to the external current. The equations of motion for the two-dimensional vortex positions  $\mathbf{r}_i$  are given by

$$\gamma_1 \frac{d\mathbf{r}_i}{dt} = - \sum_{j \neq i}^{N_v} \nabla_i V_v(\mathbf{r}_i - \mathbf{r}_j) - \sum_{k=1}^{N_p} \nabla_i V_p(\mathbf{r}_i - \mathbf{R}_k) + \mathbf{F}, \quad (2.1)$$

where  $\{\mathbf{R}_k\}$  denote the random positions of the  $N_p$  pinning centers and  $N_v$  is the total number of vortices. Here,  $\gamma_1$  is the friction coefficient of a single vortex, which will be incorpo-

rated in our unit of time. The repulsive intervortex interaction has finite range  $R_c$  and yields a force  $-\nabla V_v(r) = f_v e^{-r/R_c} (1 - r/R_c) \hat{\mathbf{r}}$  on the  $i$ th vortex, with  $R_v \leq R_c$ . The results presented below have been obtained with  $R_v = R_c$ . The second term on the right-hand side of Eq. (2.1) is the attractive pinning force of range  $R_p$ , given by  $-\nabla V_p(r) = -f_p (1 - r^2/R_p^2) \mathbf{r}/R_p$ . The range  $R_v$  of the intervortex repulsion is of the order of the superconductor penetration length  $\lambda$ , while the range  $R_p$  of the pinning potential is of the order of the superconductor coherence length  $\xi$ . In the absence of pinning the flux array forms a stable triangular lattice of lattice constant  $a_0$ .

While we have not studied in detail the dependence of our results on the shape of intervortex interaction, we believe that our findings, including the classification of the types of flow and the characterization of the plastic flow regime in terms of a bimodal distribution of vortex velocities, apply in general for any short-range intervortex interaction. The behavior could, however, be different for systems with a long-range interaction.<sup>16</sup>

One of the difficulties in carrying out a detailed numerical study of the dynamical response of this model system is the large number of parameters to be varied. In the following we have chosen the range  $R_p$  of the pinning potential as our unit of length and the maximum intervortex force  $f_v$  as our unit of force. In all cases considered the vortex lattice is rather dense, with  $n_v R_v^2 \sim 8-9$ , where  $n_v = 1/a_0^2$  is the areal density of vortices, and soft, with  $c_{66} \sim 0.271-0.334$ , where  $c_{66}$  is the shear modulus of the clean vortex lattice, in the absence of disorder. The pinning centers are modeled as point pins, in the sense that  $a_0, R_v \gg R_p$ . We have considered sets of parameters corresponding to two rather different density of pins: (i) a dense array of overlapping pins, with  $N_p/N_v = 133$  and  $n_p R_p^2 \approx 2.8$  with  $n_p$  the areal density of pins; and (ii) a dilute array of nonoverlapping pins, with  $N_p/N_v = 0.5$  and  $n_p R_p^2 \approx 0.046$ . The specific parameter values used are given below. In both cases we have varied the strength of the disorder by varying the maximum pinning force  $f_p$ .

The mean motion of the flux array is described by the drift velocity in the direction  $\hat{\mathbf{F}}$  of the driving force, given by

$$v_d(F) = \left\langle \frac{1}{N_v} \sum_{i=1}^{N_v} \mathbf{v}_i \cdot \hat{\mathbf{F}} \right\rangle. \quad (2.2)$$

The angular brackets denote the average over disorder. In the numerical calculation we average over impurity realizations by performing a time average since as time evolves the flux array samples different impurity configurations. The mean velocity is proportional to the voltage  $V$  from flux motion, while the driving force  $F$  is proportional to the driving current  $I$ . Curves of  $v_d$  versus  $F$  correspond therefore to the  $V$ - $I$  characteristics of the material.

## III. ELASTIC RESPONSE

Even in the absence of driving force the random pinning produces both elastic and plastic (dislocations) deformations of the lattice. If topological defects are explicitly forbidden in the model, the distortion induced by disorder can be described within elasticity theory.

Treating the disorder as a perturbation, it has been shown

that for  $d < 4$  order persists only in regions of linear size  $R_c$  that are pinned collectively.<sup>21</sup> The pinning length  $R_c$  can be estimated by an Imry-Ma argument<sup>22</sup> by assuming that in the presence of disorder the flux array deforms elastically to take advantage of the pinning wells. The elastic energy cost associated with displacing a region of linear size  $R$  by a distance  $R_p$  is  $\delta E_{el}(R) \sim c_{66}(R_p/R)^2 R^d$  in  $d$  dimensions, where  $c_{66}$  is the shear modulus of the flux lattice. The corresponding pinning energy gain is  $\delta E_p(R) \sim \sqrt{n_v \Gamma} (R/R_p)^{(d/2)}$  where  $\Gamma$  is the variance of the disorder potential arising from uncorrelated point pins, with  $\Gamma \approx n_p (f_p R_p^3)^2$ . For dimension  $d > 4$  the elastic energy always exceeds the pinning energy at large distances and the ordered state is stable for small disorder. For  $d < 4$  disorder dominates beyond the length  $R_c$  where the elastic strains induced by disorder are of order 1, or  $\delta E_{el}(R_c) \sim \delta E_p(R_c)$ . The elastic medium is broken up in domains of size  $R_c$ , given by

$$R_c = \frac{R_p^3 c_{66}}{\sqrt{n_v \Gamma}}, \quad (3.1)$$

in  $d = 2$ . Alternatively, the collective pinning length can be defined following Larkin and Ovchinnikov<sup>21</sup> as the length scale where the mean square displacement  $\langle [u(r)]^2 \rangle^{1/2}$  induced by disorder is of the order of the range of the pinning potential, i.e.,  $\langle [u(R_c)]^2 \rangle \sim R_p^2$ . The estimate described above neglects logarithmic corrections and assumes point pins of range  $R_p \ll a_0$ .

The Larkin-Ovchinnikov collective pinning theory applies provided  $R_c \gg a_0$ . In addition, if topological defects can occur in the lattice, the mean distance between such defects must exceed  $R_c$ . While our simulations have been carried out for parameter values where the above inequalities generally do not apply, it is useful to briefly summarize some of the properties of driven elastic media for comparison. The force needed to depin a region of linear size  $R$  can be found by equating the energy gain due to the external force  $\sim FR_p R^2$  to the pinning energy  $\delta E_p(R)$  of the region and is given by

$$F(R) \sim \frac{\sqrt{n_v \Gamma}}{R_p^2 R}. \quad (3.2)$$

In the weak pinning regime where Larkin domains of size  $R_c$  are pinned collectively by disorder, the threshold force needed to depin the medium can be estimated as the force needed to depin a Larkin domain,  $F_T^{\text{coll}} = F(R_c) \sim n_v \Gamma / (c_{66} R_p^5)$ .

When  $R_c \sim a_0$  or  $\sqrt{\Gamma}/R_p \sim c_{66} R_p^2$ , the collective pinning theory breaks down and vortices are pinned individually. In this strong pinning regime the threshold force can be estimated as  $F_T^{\text{strong}} = F(R \sim a_0) \sim n_v \sqrt{\Gamma}/R_p^2$ . The disorder-induced displacement of the lattice exceeds the range of the pinning potential and the disorder can no longer be treated as a perturbation. When this displacement becomes of order  $a_0$ , the Fourier components of the pinning potential with the periodicity of the underlying lattice become dominant and change qualitatively the nature of the pinning.<sup>23,24</sup> In this

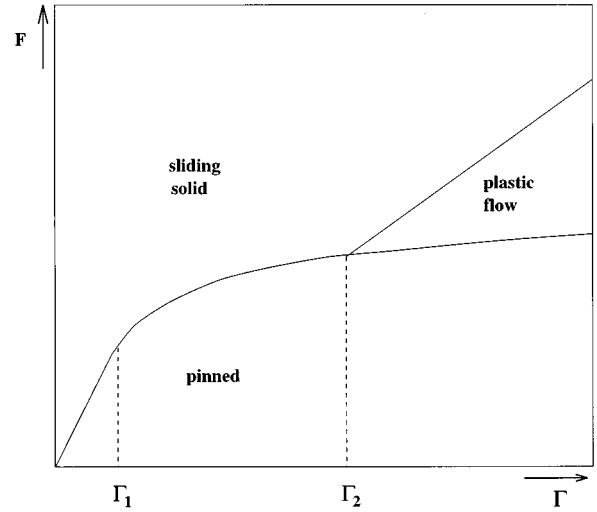


FIG. 1. A schematic ‘‘phase diagram’’ illustrating the various regimes in the  $(F-\Gamma)$  plane. The lines separating the various regions represent the estimates of threshold force discussed in the text. The boundary between pinned and sliding solid regimes is the collective threshold force  $F_T^{\text{coll}} \sim \Gamma$  for  $\Gamma < \Gamma_1 \sim (c_{66} R_p^3)^2$  and the strong pinning threshold force  $F_T^{\text{strong}} \sim \Gamma^{1/2}$  for  $\Gamma > \Gamma_1$ . For  $\Gamma > \Gamma_2 \sim (c_{66} a_0^2 R_p)^2$  there is a region of plastic flow above the pinned region, separated from the sliding solid by the force  $F_d \sim \Gamma$ .

case one needs to go beyond the simple dimensional estimates just described, as discussed recently by Giamarchi and Le Doussal.<sup>24</sup>

The question of when and how, as a function of disorder strength, topological defects proliferate has been addressed recently by Gingras and Huse<sup>19</sup> for a ferromagnetic random field XY model. Dislocations allow a region of linear size  $R$  to better adjust to disorder, yielding a gain in pinning energy. Gingras and Huse argue that a bound for the length scale  $R_d$  where dislocations proliferate can be obtained by equating the elastic energy cost of a dislocation,  $\sim c_{66} a_0^2 \ln R$ , to this pinning energy gain. If the pinning energy gain is estimated again as  $\delta E_p(R) \sim \sqrt{n_v \Gamma} R/R_p$ , we obtain  $R_d \sim (a_0^2/R_p^2) R_c$ . Notice, however, that since the disorder-induced displacements of the lattice in the presence of dislocations exceed  $R_p$ , the pinning energy no longer grows linearly with displacement and this estimate is at best a lower bound of the actual pinning energy. For this reason all we can really infer from this argument is that in the context of weak collective pinning  $R_d > R_c$ . The focus of our paper is not on determining the length  $R_d$ , but rather on the dynamics of the driven system and on the proliferation or healing of dislocations as a result of the competition between disorder, drive, and interactions. We can estimate the force needed to depin and heal dislocations separated by a length  $L_d$  as  $F_d \sim F(L_d)$ , where  $F(L)$  is given in Eq. (3.2), with the result  $F_d = n_v \Gamma / (c_{66} a_0^2 R_p^3)$ . We remark that this dimensional estimate for  $F_d$  is identical to the ‘‘crystallization’’ force  $F_t$  of Koshelev and Vinokur.

We can then distinguish three regions as a function of the disorder strength  $\Gamma$ , as shown in the schematic ‘‘phase’’ diagram of Fig. 1. These regions may or may not be separated by actual phase transitions. For  $\Gamma < (c_{66} R_p^3)^2$ ,  $L_d > L_c > a_0$

and the pinning is collective. The driven medium responds elastically and the relevant threshold force for depinning is the force  $F_T^{\text{coll}} \sim \Gamma$  needed to depin a Larkin domain. For  $(c_{66}R_p^3)^2 < \Gamma < (c_{66}a_0^2R_p)^2$ , the pinning is strong since  $L_d > a_0 > L_c$  and vortices are pinned individually. The threshold force is estimated as the force  $F_T^{\text{strong}} \sim \sqrt{\Gamma}$  needed to depin a single vortex. In both these regions the force  $F_d$  needed to depin and heal dislocations present in the lattice is smaller than the threshold force. When  $\Gamma > (c_{66}a_0^2R_p)^2$ , then  $L_d < a_0$  and the force  $F_d \sim \Gamma$  exceeds the threshold force for depinning. In this region one may have a scenario of the type proposed by Koshelev and Vinokur,<sup>11</sup> with a pinned disordered solid for  $F < F_T^{\text{strong}}$ , a region of plastic flow for  $F_T^{\text{strong}} < F < F_d$ , and finally a flowing solid with no topological defects for  $F > F_d$ .

The sliding state of an elastic medium driven through a random potential can be studied analytically via a high-velocity perturbation theory. The perturbation theory was introduced by Schmid and Hauger<sup>25</sup> and by Larkin in the context of flux lattices and further developed by Sneddon, Cross, and Fisher<sup>26</sup> for sliding CDW's. More recently Zhu, Littlewood, and Millis discussed in detail the high-velocity perturbation theory for sliding Wigner crystals.<sup>27</sup>

The starting point of the perturbation theory is a description of the flux array as an overdamped elastic continuum driven by an external force and distorted by short-range uncorrelated disorder. The equation of motion for the two-dimensional displacement field  $\mathbf{u}(\mathbf{r}, t)$  is given by

$$\gamma \partial_t \mathbf{u}(\mathbf{r}, t) = (c_{11} - c_{66}) \nabla(\nabla \cdot \mathbf{u}) + c_{66} \nabla^2 \mathbf{u} + \mathbf{F}_p(\mathbf{r}, t) + n_v \mathbf{F}, \quad (3.3)$$

where  $\gamma$  is a friction per unit area, related to the single-vortex friction coefficient of Eq. (2.1) by  $\gamma = n_v \gamma_1$ ,  $c_{11}$  and  $c_{66}$  are the compressional and shear elastic moduli of the two-dimensional flux lattice, and  $\mathbf{F}_p$  is the pinning force per unit area,

$$\mathbf{F}_p(\mathbf{r}, t) = -\rho_0(\mathbf{r}) \nabla V[\mathbf{r} + \mathbf{u}(\mathbf{r}, t)], \quad (3.4)$$

where  $\rho_0(\mathbf{r}) = \sum_{n=1}^{N_v} \delta(\mathbf{r} - \mathbf{R}_n^0)$  is the spatially inhomogeneous density of the undistorted lattice, with  $\mathbf{R}_n^0$  the sites of the triangular Abrikosov lattice. The coarse-grained quenched pinning potential  $V(\mathbf{r})$  has zero mean and short-ranged correlations,  $\langle V(\mathbf{r}) V(\mathbf{r}') \rangle = \Gamma(\mathbf{r}) f(\mathbf{r} - \mathbf{r}')$ , with  $f(r)$  a function that drops rapidly to zero for  $r \gg R_p$ . For simplicity of notation we have neglected in Eq. (3.4) the nonlocality of the elastic constants. This can, however, be easily incorporated in the perturbation theory. The drift velocity is defined here as  $v_d(F) = \langle \partial_t \mathbf{u} \cdot \hat{\mathbf{F}} \rangle$ , where the brackets denote a spatial average, as well as a disorder average. In the absence of disorder  $v_d(F) = F/\gamma$ . Treating the disorder as a perturbation relative to the external driving force, one can then evaluate corrections to this uniformly sliding state. The details of the calculation are not given here as this follows closely the perturbation theory for the Wigner crystal described recently by Zhu *et al.*<sup>27</sup> Rather than expanding about the solution  $v_d(F) = F/\gamma$  in the absence of disorder, one actually constructs a self-consistent perturbation theory by writing  $\mathbf{u}(\mathbf{r}, t) = v_d t \hat{\mathbf{F}} + \mathbf{s}(\mathbf{r}, t)$ , solving for  $\mathbf{s}(\mathbf{r}, t)$  in perturbation

theory and then requiring  $\langle \partial_t \mathbf{s}(\mathbf{r}, t) \rangle = 0$ . The lowest nonvanishing correction  $\delta v_d = v_d - F/\gamma$  to the mean velocity is given by

$$\delta v_d(F) \approx -\frac{n_v^2}{2\gamma G \neq 0} \sum \Gamma(G) G^2 (\mathbf{G} \cdot \hat{\mathbf{F}}) \times \int_{\text{BZ}} \frac{d\mathbf{k}}{(2\pi)^2} \frac{\gamma \mathbf{v} \cdot \mathbf{G}}{(c_{66}k^2)^2 + (\gamma \mathbf{v} \cdot \mathbf{G})^2}, \quad (3.5)$$

where  $\mathbf{G}$  are the reciprocal lattice vectors of the triangular flux lattice and the  $\mathbf{k}$  integral is over the first Brillouin zone of size  $k_{\text{BZ}} = \sqrt{4\pi n_v}$ . The disorder correlator is given by  $\Gamma(\mathbf{G}) \approx \Gamma \approx n_p (f_p R_p^3)^2$ , for  $G < 1/R_p$ , and vanishes rapidly for  $G \gg 1/R_p$ . It therefore cuts off the reciprocal lattice vectors sum at  $G_{\text{max}} \sim 1/R_p$ . For the case of point pins ( $a_0 \gg R_p$ ), the right-hand side of Eq. (3.5) can be evaluated exactly by transforming the wave vector sum to an integral. It is, however, more instructive to present the result in two limiting cases. If the velocity is not too large,  $v_d \ll c_{66} k_{\text{BZ}}^2 R_p / \gamma$ , the main contribution to the  $\mathbf{k}$  integral comes from the small- $k$  region, corresponding to length scales much larger than the range of the pinning potential. The upper limit of the wave vector integral can be extended to infinity, with the result

$$\delta v_d(F) \approx -\frac{n_v}{4\gamma c_{66} G \neq 0} \sum \Gamma(G) G^2 \mathbf{G} \cdot \hat{\mathbf{F}} \text{sgn}(\mathbf{G} \cdot \mathbf{v}_d) \approx -\frac{\Gamma n_v}{4\gamma c_{66} R_p^5}. \quad (3.6)$$

In this intermediate-velocity regime the lifetime of elastic deformations of the sliding medium is small compared to the time to cross the range of the pinning potential, yielding collective pinning of the lattice. For the two-dimensional case considered here in this regime one obtains a force-independent correction to the drift velocity. Conversely, if  $v_d \gg c_{66} k_{\text{BZ}}^2 R_p / \gamma$ , the time needed to cross the range of the pinning potential—and therefore to see uncorrelated disorder—is short compared to the lifetime of elastic deformations connecting neighboring vortices, and one obtains single particle response, with

$$\delta v_d(F) \approx -\frac{\Gamma}{16\pi \gamma_1 R_p^4} \frac{1}{F}. \quad (3.7)$$

Notice that the coefficient of  $1/F$  in Eq. (3.7) is indeed independent of vortex density.

#### IV. NUMERICAL RESULTS

We have performed molecular dynamics simulations of arrays of 300, 920, and 1200 vortices using periodic boundary conditions. The results presented below are for two sets of parameter values, unless otherwise specified. The data for the array with a dilute concentration of pins ( $N_p/N_v = 0.5$ ) are obtained with  $N_v = 920$ ,  $N_p = 460$ , and  $R_v = 9.9$ . For these parameter values the clean Abrikosov lattice has lattice constant  $a_0 = 3.54$ , with  $n_v R_v^2 = 9.0$ , and shear modulus  $c_{66} = 0.271$ . As discussed earlier, all lengths are measured in units of  $R_p$  and forces are in units of  $f_v$ . The data for the densely pinned array ( $N_p/N_v = 133$ ) are obtained with

TABLE I. Collective pinning lengths and estimated threshold forces for the values of the pinning force used in the simulations.

$f_p$	$N_p/N_v=0.5$			$N_p/N_v=133$		
	$R_c/a_0$	$F_T^{\text{est}}$	$f_p$	$R_c/a_0$	$F_T^{\text{est}}$	
0.2	20.0	$2.1 \times 10^{-4}$	0.03	7.8	$1.4 \times 10^{-4}$	
0.5	13.3	$1.3 \times 10^{-3}$	0.1	2.3	$1.6 \times 10^{-3}$	
1.0	4.0	$5.3 \times 10^{-3}$	0.3	0.8	$1.0 \times 10^{-2}$	
1.5	2.7	$1.2 \times 10^{-2}$	3.0	0.08	$1.0 \times 10^{-1}$	
2.0	2.0	$2.1 \times 10^{-2}$				

$N_v=300$ ,  $N_p=40\,000$ , and  $R_v=20$ . In this case  $a_0=7.44$ , with  $n_v R_v^2=8.3$ , and  $c_{66}=0.334$ . Table I shows the values of the collective pinning length  $R_c$  given in Eq. (3.1) and the threshold force estimated using the dimensional analysis discussed in Sec. III for various pinning forces  $f_p$ . For each set of parameters the value of the threshold force given in the table is the smaller of the two estimates  $F_T^{\text{coll}}$  and  $F_T^{\text{strong}}$ .

The drift velocity of the vortex array is shown as a function of driving force in Figs. 2(a) and 3(a) for various values of the maximum pinning force  $f_p$ . Figure 2 is for the sample with a low concentration of pins ( $N_p/N_v=0.5$ ), while Fig. 3 is for the densely pinned sample ( $N_p/N_v=133$ ). Figures 2(b) and 3(b) display the differential resistivity  $dv_d/dF$ . Both Figs. 2(a) and 3(a) show a systematic evolution of the shape of the  $V$ - $I$  curve with increasing disorder strength not unlike that observed in the  $V$ - $I$  curves of real superconductors.<sup>6</sup> For small pinning forces the velocity is nonlinear in  $F$  only very near threshold, where it exhibits a very small region of negative curvature. Correspondingly, there is no peak in the differential resistivity. At larger pinning forces there is a change in the sign of the curvature of the mean velocity that occurs at a value  $F_{\text{peak}}$  above threshold, but well in the nonlinear region, and yields a peak in the differential resistivity. The location of this peak moves to larger driving forces as the pinning force increases. This dependence is particularly strong in the sample with a dense pin array. For  $F > F_{\text{peak}}$  the  $V$ - $I$  characteristic is concave down and as  $F$  grows it approaches the asymptotic value  $v_d=F$ , corresponding to a freely sliding array. In this region the deviations from the linear behavior  $v_d=F$  are fit *quantitatively* by the single-particle perturbation theory result given in Eq. (3.7). This can be rewritten as  $v_d/F \approx 1 - \langle F_p^2(0) \rangle / F^2$ , where  $\langle F_p^2(0) \rangle = \Gamma / R_p^2$  is the mean square total pinning force. For the specific pinning potential used in our simulations,  $\langle F_p^2(0) \rangle = (\pi/30)n_p R_p^2 f_p^2$ . The rms velocity fluctuations defined as  $v_{\text{rms}} = \langle [(1/N)\sum_i \mathbf{v}_i \cdot \hat{\mathbf{F}} - v_d]^2 \rangle^{1/2}$  are also fit quantitatively by their single-particle value,  $v_{\text{rms}} = [\langle F_p^2 \rangle / 2N_v]^{1/2}$  in this region. We stress that for very strong pinning the flux array can be very disordered even in the region  $F > F_{\text{peak}}$ , with sometimes as much as 50% of the vortices with a coordination number different from 6 [see Fig. 4(b) below]. This is because dislocations can be frozen in the sliding lattice in our  $T=0$  simulations, yielding a disordered array that slides as a whole, with dislocations moving along at the same velocity as the rest of the lattice. This behavior may be a finite-size effect and is related to the hysteresis in the defect configuration discussed below.

For  $N_p/N_v=0.5$  the threshold force remains very small

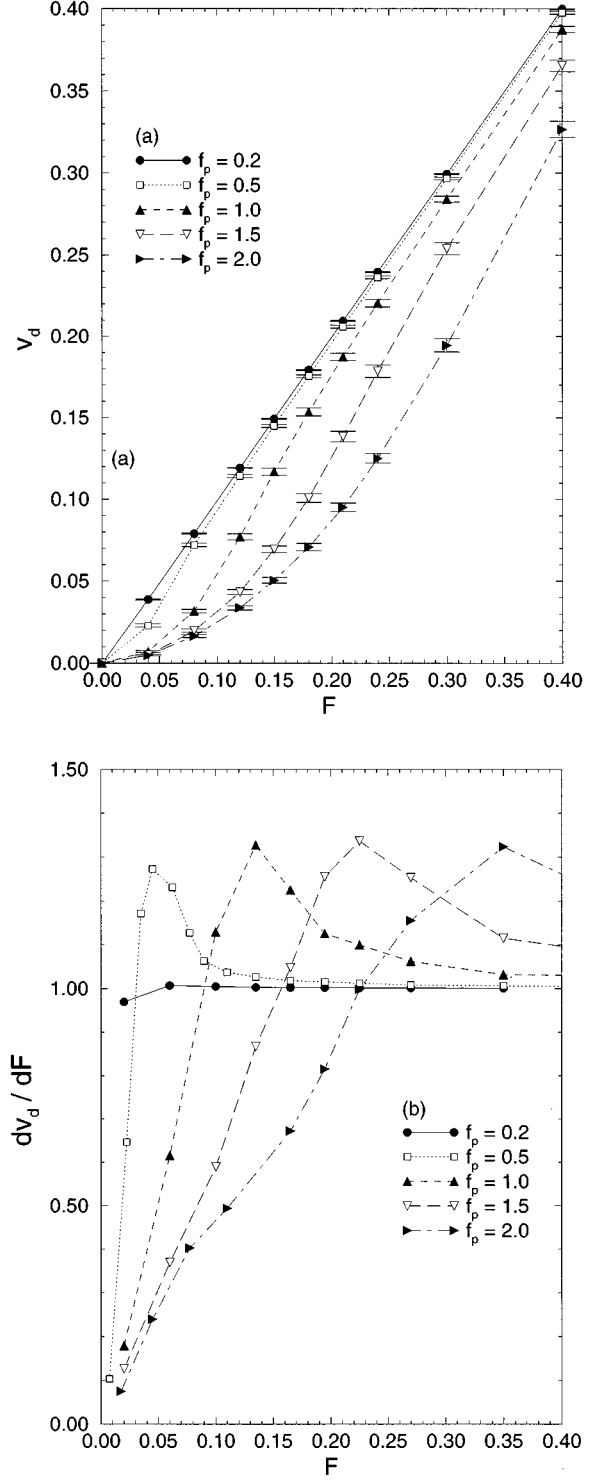


FIG. 2. Drift velocity (a) and differential resistivity  $dv_d/dF$  (b) vs driving force for the array with a dilute distribution of pinning centers,  $N_p/N_v=0.5$ . The curves obtained by ramping the force up and down are indistinguishable. The error bars represent the value of  $v_{\text{rms}}$ .

for all values of the pinning force studied. We cannot exclude that the threshold force may vanish in this case, but we have not performed extensive runs near threshold and finite-size scaling to determine the location of the threshold precisely. In fact, for a model with dislocations, it is not necessary that  $F_T \neq 0$  at zero temperature ( $T=0$ ). In contrast, the

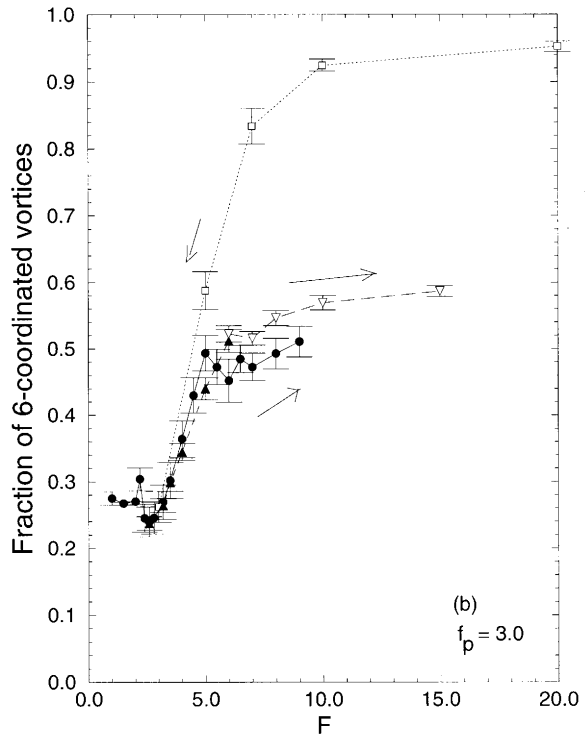
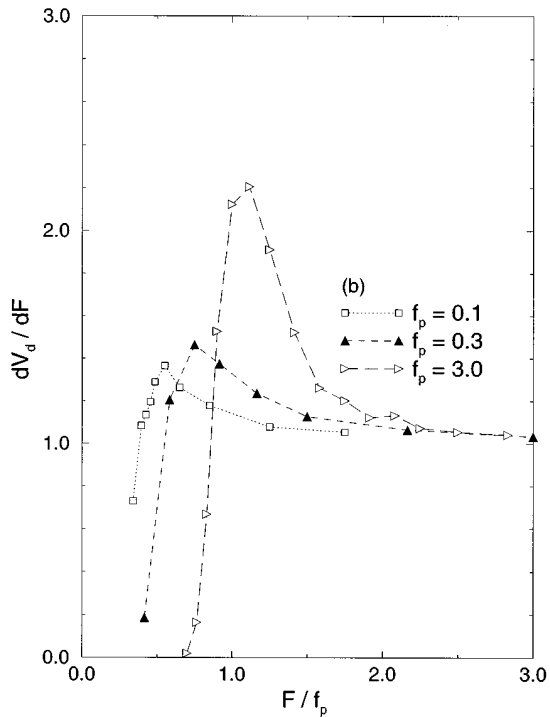
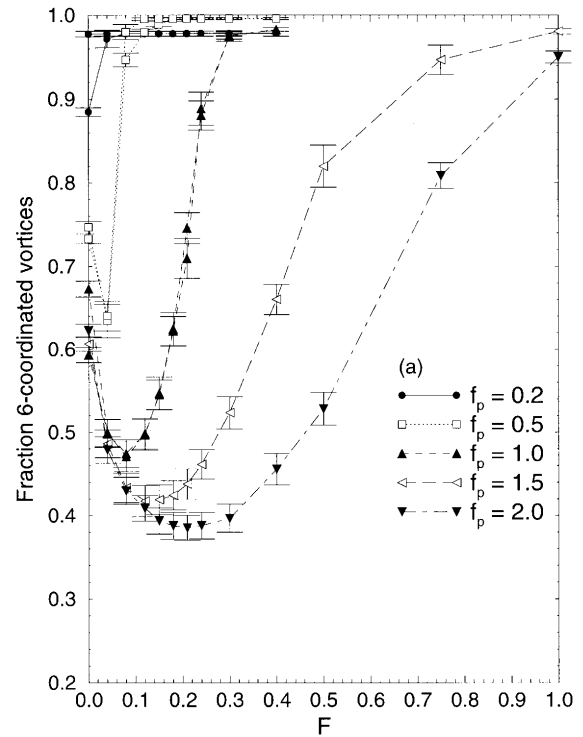
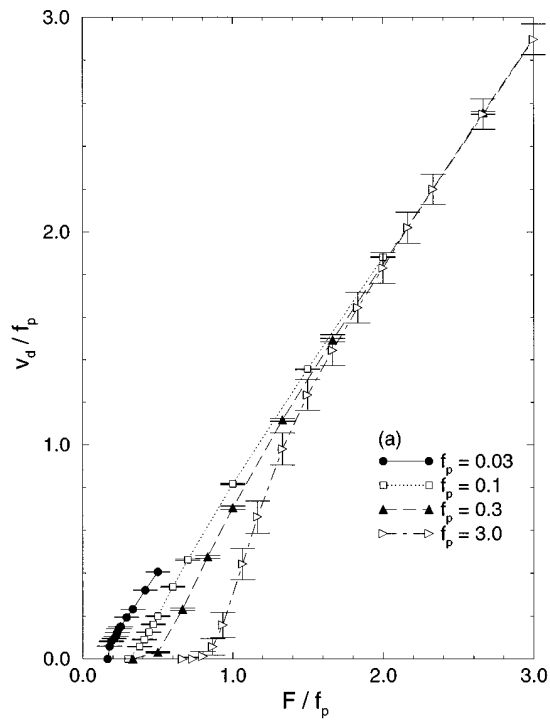


FIG. 3. Drift velocity (a) and differential resistivity  $dv_d/dF$  (b) vs driving force for the array with a dense distribution of pinning centers,  $N_p/N_v = 133$ . The curves obtained by ramping the force up and down are indistinguishable. The error bars represent the value of  $v_{rms}$ . Notice that both  $v_d$  and  $F$  have been divided by  $f_p$  to display the data obtained for different values of the pinning force on the same graph.

threshold force is large and clearly nonzero for  $N_p/N_v = 133$ . While we have not determined the threshold value accurately, we find that the numerical estimate agrees in order of magnitude with the dimensional estimates given

FIG. 4. Fraction of sixfold coordinated vortices vs driving force. (a) is for  $N_p/N_v = 0.5$  and the parameter values of Fig. 2. In this case the curves obtained by ramping the force up and down are virtually indistinguishable and no hysteresis is observed. (b) is for  $N_p/N_v = 133$ , with the parameter values of Fig. 3 and  $f_p = 3.0$ . The lower curves are obtained by ramping up the force from an initial disordered configuration of the flux array. Data for both  $N_v = 300$  (circles) and  $N_v = 1200$  (triangles) are shown to display the finite-size effect. The upper curve (square) is obtained by ramping down the force from an initial ordered configuration with  $N_v = 300$ .

in Table I. Our numerical  $V$ - $I$  characteristics resemble those obtained in earlier simulations of the same model.<sup>7,8,11</sup> There is, however, an important difference between our results and those of Koshelev and Vinokur<sup>11</sup> in that we see no hysteresis in the  $V$ - $I$  characteristics other than that arising from finite-size effects. For small systems, we do see hysteresis in the  $V$ - $I$  curves similar to that reported by Koshelev and Vinokur, but this hysteresis vanishes in larger systems. This hysteresis may be due to the periodic boundary conditions, which lead to metastable periodic attractors for the dynamics. The hysteresis in small systems in our simulations is associated with such periodic attractors.

We have also studied the evolution of the number of defects in the lattice with driving force. In most of our runs the flux array is prepared in an initial random disordered configuration and the driving force is then ramped up from zero. We have tracked the defects in the lattice by doing Voronoi constructions during the run and counting the number of vortices that are not sixfold coordinated. The fivefold and sevenfold coordinated vortices are disclinations in the two-dimensional triangular flux lattice and, when paired, correspond to a dislocation. Figure 4(a) shows the time averaged fraction of sixfold coordinated vortices as a function of the driving force for  $N_p/N_v=0.5$ . In looking at these curves it should be kept in mind that the number of defects present at  $F=0$  depends on initial conditions and the realization of disorder. As observed earlier,<sup>11</sup> we find that the flux array orders at large driving force. The value of the driving force where the number of defects starts dropping is of the order of the location of the peak in the differential resistivity. Again, we have observed no hysteresis in the number of defects for the sample with a low concentration of pins other than one arising from finite-size effects. We do, however, find hysteresis in the number of defects when the disorder is very strong, as shown in Fig. 4(b). In this case when we ramp-up the force from an initial disordered vortex configuration, defects get “frozen in” and the lattice never orders. Starting from an ordered configuration at high fields, the lattice maintains its order. We have not been able to exclude that this hysteresis is also a finite-size effect. We expect that this hysteresis will disappear in the presence of thermal fluctuations. The value of the driving force where the defects become frozen in apparently corresponds to the onset of the single particle behavior discussed below.

In order to correlate the macroscopic response of the vortex array with the details of the microscopic vortex motion, we have performed a variety of visualizations and we have studied the spatial distribution of vortex velocities. One method of displaying the data that we have found useful is to plot histograms of the component of the vortex velocity in the direction of the driving force ( $x$  component). Figure 5 shows the evolution of such histograms of the  $x$  component of the *instantaneous* vortex velocity near threshold with driving force for parameter values that yield crinkle flow. For all driving forces, the histograms have a single maximum at a value of velocity close to the mean drift velocity. The location of the maximum moves to larger velocities as the driving force increases. Very close to threshold, velocities are distributed asymmetrically about the mean value and the histograms are not unlike those obtained from a phase-only model of CDW's.<sup>28</sup> As the driving force increases the veloc-

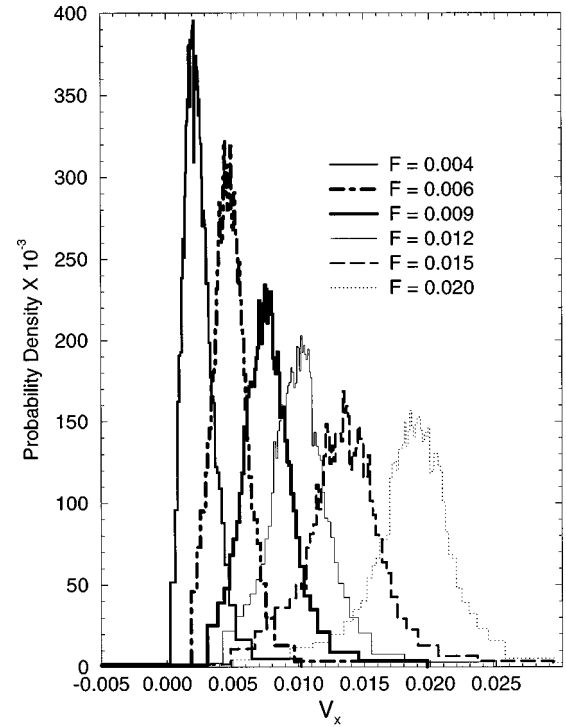


FIG. 5. Evolution of histograms of instantaneous velocity  $v_x$  with applied driving force for the parameters of Fig. 2 and  $f_p=0.2$ . The system exhibits crinkle flow near threshold.

ity distribution becomes sharper and symmetric.

The instantaneous velocity distributions are quite different for parameter values where plastic flow is found. In this case the velocity histograms display a clear bimodal structure near threshold, as shown in Fig. 6, indicating the presence of two distinct “typical” velocities of the vortices. The first peak, which is approximately centered at zero very near threshold, is determined by the “slow” vortices in the array, located in pinned or temporarily pinned regions. This peak has finite width due to the oscillations of the “slow” or pinned vortices about the pins due to interactions with vortices flowing nearby. The peak at larger velocity is determined by the “fast” vortices that flow in channels around the pinned regions. We stress, however, that individual vortices are sometimes “slow,” sometimes “fast.”

As a result of the temporal fluctuations in the velocity, we expect a large voltage noise in this region, perhaps related to the experiments by Marley, Higgins, and Bhattacharya.<sup>6</sup> The various curves correspond to different driving forces, ranging from close to threshold (the threshold force for this case is estimated as  $F_T \sim 5.3 \times 10^{-3}$ ) to well within the linear regime. The bimodal structure disappears at a value of  $F$  close to the location  $F_{\text{peak}}$  of the peak of the differential resistivity (here  $F_{\text{peak}} \sim 0.125$ ). Beyond this value the  $V$ - $I$  curve rapidly becomes linear and the velocity distribution is narrow and symmetric, centered at the mean velocity. The origin of the maximum in the differential resistivity can easily be traced back to the shape of the velocity histograms by studying the location of the two peaks and their relative weights (Fig. 7) as functions of the driving force. Using a crude approximation, we can write the drift velocity of the vortex array as  $v_d = n_s v_s + n_f v_f$ , where  $n_s$  and  $n_f$  are the fraction of slow

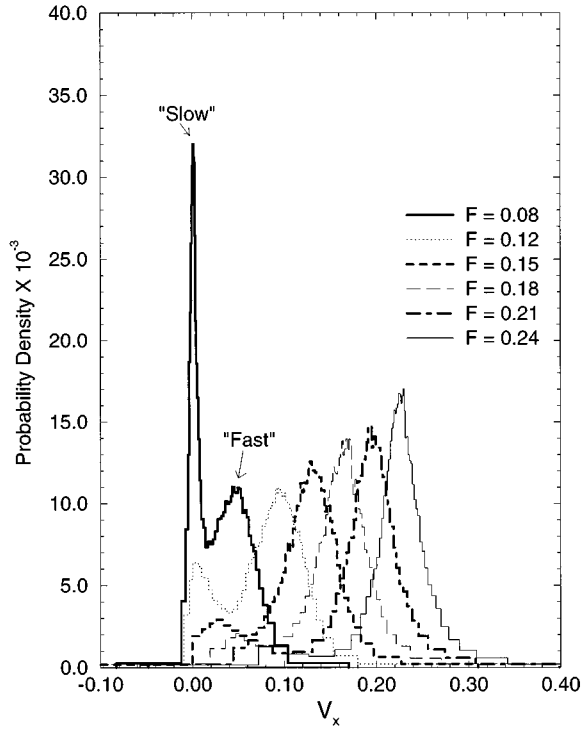


FIG. 6. Evolution of the histograms of instantaneous velocity  $v_x$  with applied force for the parameter values of Fig. 2 and  $f_p = 1$ . The system exhibits plastic flow near threshold and the histograms clearly display a bimodal structure in this region.

and fast vortices, respectively, identified with the area under the respective peaks of the velocity distribution and shown in Fig. 7(b). Similarly,  $v_s$  and  $v_f$  are the corresponding velocities, identified here with the location of the two peaks and displayed in Fig. 8(a). Using  $n_s + n_f = 1$ , we obtain  $(dv_d/dF) \approx dv_f/dF + (dn_f/dF)(v_f - v_s)$ . For  $F < F_{\text{peak}}$  the slow vortices are essentially not moving ( $v_s \approx 0$ ) while the number  $n_f$  of fast vortices is increasing rapidly, leading to a superlinear  $V$ - $I$ . Above  $F_{\text{peak}}$  the rate  $dn_f/dF$  at which the slow vortex fraction increases slows down considerably, while  $(v_f - v_s) \sim F$ —it is this slowing down of the rate  $dn_f/dF$  with increasing  $F$  that is responsible for the peak in the differential resistivity.

The bimodal structure of the velocity histograms discussed above reflects the spatial inhomogeneity of the instantaneous vortex velocity. A crucial question for the characterization of plastic flow is whether or not this bimodal structure will persist when the vortex velocity is time averaged over times larger than those corresponding to an average displacement of the lattice of at least a lattice constant. It has been suggested that an important distinction between plastic and elastic response can be found in the correlations of the time-averaged velocity.<sup>6</sup> Indeed, in a model where dislocations are forbidden and the response is therefore elastic, the time-averaged velocity will be spatially homogeneous and correlated over the entire system size. In contrast, in a system exhibiting plastic flow the time-averaged local velocity should still be spatially inhomogeneous, yielding bimodal structure of the corresponding histogram. We have constructed histograms of time-averaged vortex velocities, defined as  $\bar{v}_i(T) = \int_0^T (dt/T)v_i(t)$  for various values of  $T$ ,

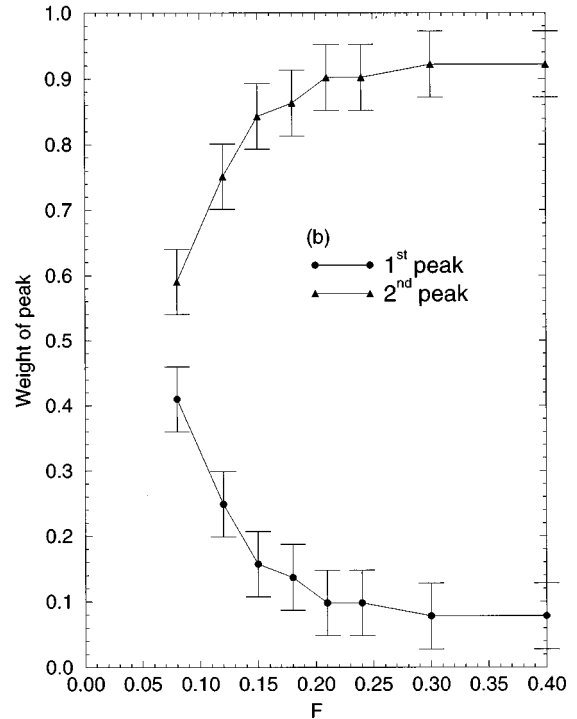
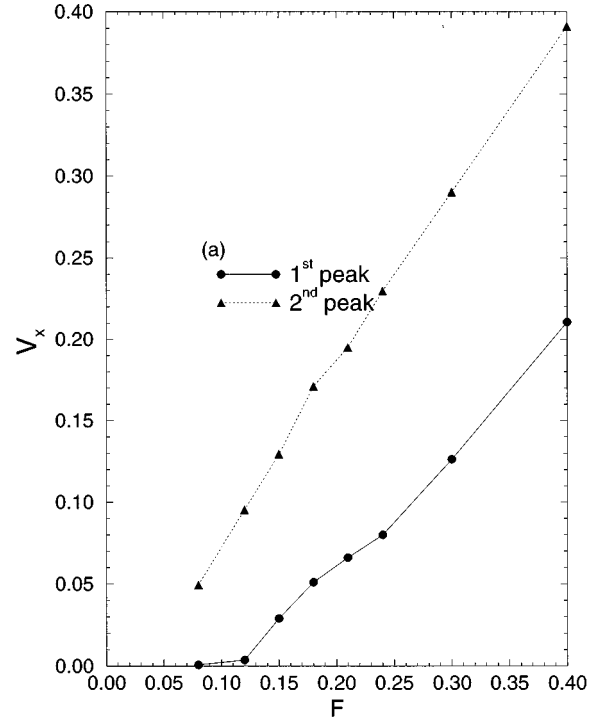


FIG. 7. These figures display the evolution with applied force of the location (a) and weights (b) of the peaks of the histograms of Fig. 6. The location is obtained by recording the velocities at which each peak is maximum. The weight of the first peak is the ratio of the area under the part of the histogram up to the minimum between the two peaks, to the total area under the curve. The weight of the second peak is 1, the weight of the first peak.

where  $T=1$  yields the histogram of instantaneous velocity discussed above. The histograms are shown in Fig. 8 for two values of the driving force. The bimodal structure clearly remains for the time-averaged velocities.



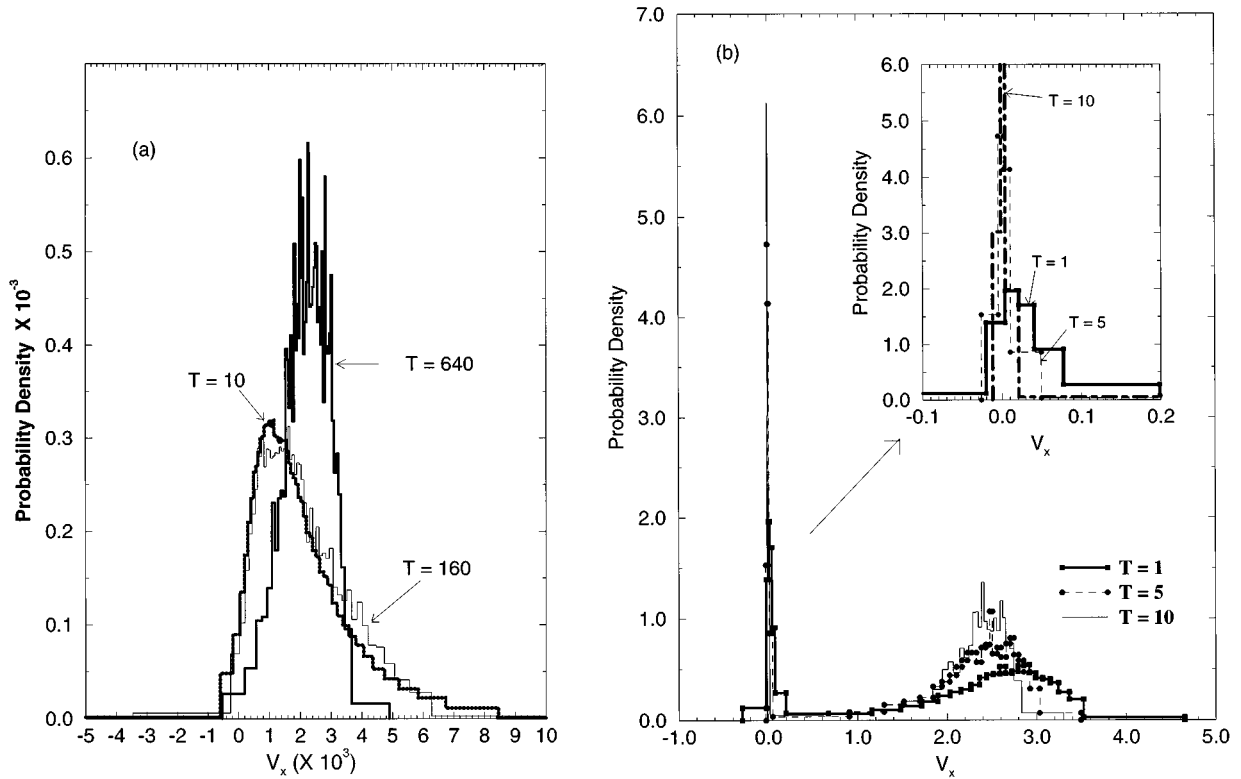


FIG. 8. These figures compare histograms of *instantaneous* and *time-averaged* vortex velocities. The vortex velocities are averaged over a time  $T$ . The value  $T=1$  yields the instantaneous velocity histograms of Figs. 5 and 6. (a) corresponds to parameter values yielding ‘‘crinkle’’ flow (same as Fig. 3 for  $f_p=0.03$  and  $F=0.0054$ ). In this case the instantaneous velocity histogram exhibits a single maximum near  $v_d \sim 0.001$  and is essentially identical to the histogram obtained with  $T=10$  and  $T=160$ . Notice that in a time  $T=10$  the vortices displace on the average a distance  $\Delta x \sim 0.018a_0$ . The histogram for  $T=640$  is sharper, but qualitatively unchanged, indicating that the system motion is well correlated for these parameter values. The histograms shown in (b) refer to parameter values yielding plastic flow (same as Fig. 3 for  $f_p=3$  and  $F=3.5$ ). In this case the histogram of instantaneous velocities ( $T=1$ , solid curve) has a bimodal structure, which persists upon time averaging ( $T=5$  or  $\Delta x \sim 1.4a_0$  and  $T=10$  or  $\Delta x \sim 2.7a_0$ ), indicating a true plastic response.

To summarize, our model of a two-dimensional flux array driven through quenched disorder exhibits two types of response. For very weak disorder strength, the flux array exhibits ‘‘crinkle’’ motion, with correlated patches of vortices making small forward jumps at different times, like a tablecloth being pulled on a rough surface. At very small driving forces the lattice contains an appreciable number of fivefold and sevenfold disclinations. The defects are concentrated at the boundaries between the patches with correlated velocities and their number drops rapidly to zero with increasing driving force. The distribution of vortex velocities displays a single maximum at a value of the velocity of the order of the mean velocity of the array (Fig. 3). As the driving force is increased and the flux array gets depinned, the maximum shifts to a higher velocity and the distribution broadens with no substantial change in shape. The histograms of time-averaged velocities become sharper as the averaging time increases and stop changing once the averaging time exceeds the time over which the vortex lattice advances on the average a distance of a few  $R_p$ . This type of response is similar to that observed by Hu and Westervelt in magnetic bubble arrays.<sup>20</sup> These authors report observing a bimodal velocity distribution, but this is because they only look at the distribution of velocity over a very small time scale, smaller than the time required for the array as a whole to advance a distance of the order of the range of the pinning potential. Hu

and Westervelt also argue that the response exhibits scaling in this regime. While we have not studied in sufficient detail the region near threshold to observe scaling, it seems quite plausible that this ‘‘crinkle’’ regime will exhibit generic critical behavior, analogous to that predicted and observed for an elastic medium, in spite of the presence of defects. The fairly large number of defects present in our system at very small driving forces may very well be an artifact of our initial conditions, with vortex positions chosen at random, rather than equilibrated. It may be that if a low but finite temperature is introduced in the model and the flux array is initially allowed to equilibrate in the presence of the disorder, the number of defects present for the parameter values yielding crinkle motion would be practically negligible even at the smallest driving forces.

In most of the region of parameter space studied we have observed plastic flow of the flux array. This regime is characterized macroscopically by a change in the sign of the curvature of the  $V$ - $I$  characteristic well above threshold, which yields a maximum in the differential resistance  $dv_d/dF$ , and by a large number of defects in the region below the maximum. The flow is spatially inhomogeneous. Over a short time interval one observes fluidlike flow of moving regions around pinned regions. On the average, however, all vortices participate in the motion in the sliding state and no regions of the array are stuck for the entire length of

the simulation, even near threshold. The evolution of the velocity distribution with driving force is shown in Fig. 4. There is clearly a bimodal velocity distribution in the sliding state which persists until all defects have healed and the  $V-I$  has become linear. A single vortex is in general “slow” for some of the time and “fast” for some of the time. This should result in a large voltage noise, as observed by Marley, Higgins, and Bhattacharya.<sup>6</sup>

As the pinning force is increased, the persistence time of this structure of pinned and flowing regions grows and pinned vortices remain pinned for longer and longer times. For the situation of strongest pinning among those studied ( $f_p=3$  for  $N_p/N_v=300$ ), we find that some vortices are pinned for the entire length of the simulations, while others are flowing quite freely in channels surrounding the pinned regions. In this case the structure of the channels is time independent near threshold. As the driving force is increased all vortices are eventually depinned and the  $V-I$  becomes linear. The array is very defective near threshold and the velocity distribution is bimodal and remains bimodal when velocities are time averaged. The flux array displays a filamentary motion similar to that observed by Middleton and Wingreen for an array of quantum dots,<sup>29</sup> where near threshold the current flows in a single narrow channel and exhibits critical scaling. Critical scaling was also predicted in a model of fluid flow down a rough incline by Narayan and Fisher.<sup>9</sup> In this case again the flow pattern consists of directed channels that run across the system. It may be that in this very strong pinning regime the driven flux array also exhibits generic critical behavior, not unlike that of the fluid model of Ref. 9.

Some insight into the parameter regions where the two regimes described above may be expected to occur can be

gained by considering the Larkin-Ovchinnikov pinning length, given in Table I for the case where the range  $R_p$  of the pinning potential is small compared to both  $R_v$  and  $a_0$ . If  $R_v \gg a_0$ , the shear modulus of the flux array can be estimated as  $c_{66} \sim f_v R_v / a_0^2$  and  $L_c \sim R_v f_v \sqrt{N_v} / (f_p \sqrt{N_p})$ . The flux array should therefore be pinned collectively ( $L_c \gg a_0$ ) provided  $f_v \sqrt{N_v} / (f_p \sqrt{N_p}) > 1$ . We find that these inequalities are generally satisfied in the cases where we observe a crinkle response. Conversely, when  $f_v \sqrt{N_v} / (f_p \sqrt{N_p}) \ll 1$ , even if  $R_v \gg a_0$ , we obtain  $L_c \sim a_0$  and vortices can be pinned individually, yielding plastic flow or eventually filamentary flow. A transition between these two regimes is indeed observed as  $f_p$  is increased for the parameter values discussed above (here  $L_c$  decreases over almost two orders of magnitudes over the range of pinning forces studied, from  $L_c \sim 20a_0$  for  $f_p=0.2$  to  $L_c \sim 0.3a_0$  for  $f_p=10$ ). Using again the above estimate for  $c_{66}$  for  $R_v \gg a_0$  we find that in the collective pinning regime the threshold force needed to depin the array is given by  $F_T \sim (N_p/N_v)(R_p/R_v)(f_p^2/f_v)$ . The increase of the threshold force with  $f_p$  observed in Fig. 2(a) is consistent with this dependence.

#### ACKNOWLEDGMENTS

It is a pleasure to acknowledge helpful conversations with Shobo Bhattacharya. This work was supported by the National Science Foundation at Syracuse through Grant Nos. DMR-9217284 and DMR-9419257, and at the ITP of the University of California in Santa Barbara through Grant No. PHY-8904035. A.A.M. thanks the Alfred P. Sloan foundation for support. Finally, we thank Ki-Ho Lee for help with the numerical work in the early stages of this work.

- 
- <sup>1</sup>G. Blatter *et al.*, Rev. Mod. Phys. **66**, 1125 (1994).  
<sup>2</sup>M.A. Rubio *et al.*, Phys. Rev. Lett. **63**, 1685 (1989); N. Martys, M. Cieplak, and M.O. Robbins, *ibid.* **66**, 1058 (1991).  
<sup>3</sup>G. Grüner, Rev. Mod. Phys. **60**, 1129 (1988).  
<sup>4</sup>D.S. Fisher, Phys. Rev. B **31**, 1396 (1985).  
<sup>5</sup>S.N. Coppersmith, Phys. Rev. Lett. **65**, 1044 (1990); S.N. Coppersmith and A.J. Millis, Phys. Rev. B **44**, 7799 (1991).  
<sup>6</sup>S. Bhattacharya and M.J. Higgins, Phys. Rev. Lett. **70**, 2617 (1993); Phys. Rev. B **49**, 10 004 (1994); A.C. Marley, M.J. Higgins, and S. Bhattacharya, Phys. Rev. Lett. **74**, 3029 (1995); M.J. Higgins and S. Bhattacharya, Physica C **257**, 232 (1996).  
<sup>7</sup>H.J. Jensen, A. Brass, Y. Brechet, and A.J. Berlinsky, Phys. Rev. B **38**, 9235 (1988); H.J. Jensen, in *Phase Transitions and Relaxation in Systems with Competing Energy Scales*, Vol. 415 of *NATO Advanced Study Institute, Series C*, edited by T. Riste and D. Sherrington (Kluwer Academic Publishers, Dordrecht, 1993), p. 129, and references therein.  
<sup>8</sup>A.-C. Shi and A.J. Berlinsky, Phys. Rev. Lett. **67**, 1926 (1991).  
<sup>9</sup>O. Narayan and D.S. Fisher, Phys. Rev. B **49**, 9469 (1994).  
<sup>10</sup>A.E. Koshelev, Physica C **198**, 371 (1992).  
<sup>11</sup>A.E. Koshelev and V.M. Vinokur, Phys. Rev. Lett. **73**, 3580 (1994).  
<sup>12</sup>L. Balents and M.P.A. Fisher, Phys. Rev. Lett. **75**, 4270 (1995).  
<sup>13</sup>X.S. Ling and J. Budnick, in *Magnetic Susceptibility of Superconductors and Other Spin Systems*, edited by R.A. Hein, T.L. Francavilla, and D.H. Liebenberg (Plenum, New York, 1991).  
<sup>14</sup>W.K. Kwok *et al.*, Phys. Rev. Lett. **72**, 1092 (1994); **73**, 2614 (1994).  
<sup>15</sup>W. White, A. Kapitulnik, and M. Beasley, Phys. Rev. B **50**, 6303 (1994).  
<sup>16</sup>N. Gronbech-Jensen, A.R. Bishop, and D. Dominguez, Phys. Rev. Lett. **76**, 2985 (1996).  
<sup>17</sup>M.-C. Cha and H.A. Fertig, Physica B **50**, 14 368 (1994).  
<sup>18</sup>D. Huse (unpublished).  
<sup>19</sup>M. Gingras and D. Huse, Phys. Rev. B **53**, 15 193 (1996).  
<sup>20</sup>J. Hu and R. M. Westervelt, Phys. Rev. B **51**, 17 279 (1995).  
<sup>21</sup>A.I. Larkin and Yu.N. Ovchinnikov, Zh. Éksp. Teor. Fiz. **65**, 1704 (1973) [*Sov. Phys. JETP* **38**, 854 (1974)].  
<sup>22</sup>Y. Imry and S.-K. Ma, Phys. Rev. Lett. **35**, 1399 (1975).  
<sup>23</sup>T. Nattermann, Phys. Rev. Lett. **64**, 2454 (1990).  
<sup>24</sup>T. Giamarchi and P. Le Doussal, Phys. Rev. B **52**, 1242 (1995).  
<sup>25</sup>A. Schmid and W. Hauger, J. Low Temp. Phys. **11**, 667 (1973).  
<sup>26</sup>L. Sneddon, M. Cross, and D.S. Fisher, Phys. Rev. Lett. **49**, 292 (1982).  
<sup>27</sup>X. Zhu, P.B. Littlewood, and A.J. Millis, Phys. Rev. B **50**, 4600 (1994).  
<sup>28</sup>S.N. Coppersmith and D.S. Fisher, Phys. Rev. A **38**, 6338 (1988).  
<sup>29</sup>A.A. Middleton and N.S. Wingreen, Phys. Rev. Lett. **71**, 3198 (1993).